44th AIAA Aerospace Sciences Meeting and Exhibit
9 - 12 January 2006, Reno, Nevada

AIAA 2006-1055

Optimization of Unstalled Pitching and Plunging Motion of an Airfoil

Shuchi Yang*, Shijun Luo†, Feng Liu‡
Department of Mechanical and Aerospace Engineering
University of California, Irvine, CA 92697-3975
Her-Mann Tsai§
Temasek Laboratories
National University of Singapore
Kent Ridge Crescent, Singapore 119260

The motion parameters of a sinusoidally pitching and plunging NACA 0012 airfoil in a uniform stream of low speeds are optimized for high propulsive efficiency and/or high time-averaged thrust coefficient by the inviscid version of a three-dimensional unsteady compressible Euler/Navier-Stokes flow solver. A limited maximum effective angle of attack is applied on the optimization to ensure fully attached flow. Preliminary optimization is obtained by means of the classical linear theory, and then refined optimization is performed by the Euler computation. The highest inviscid propulsive efficiency of 90% with a time-averaged inviscid thrust coefficient of 0.24, and the highest inviscid thrust coefficient of 0.86 with a propulsive efficiency of 65% are obtained at the freestream Mach number of 0.1 and zero mean angle of attack. The mean angle of attack has little effect on the time-averaged thrust coefficient and the propulsive efficiency and can be ignored in the optimization.

I. Introduction

It is known that the flapping motion of bird flight is a coupled pitching and plunging oscillation with some phase difference between them. Pure plunging oscillation is capable of producing thrust with high propulsive efficiency. However, the large plunging velocity may induce flow separation which would degrade the efficiency significantly. Pure pitching oscillation alone is not an efficient motion, but when coupled with a plunging oscillation with appropriate phase shift it can suppress the flow separation and high propulsive efficiency can be obtained. At present, many projects are devoted to developing air and water vehicles which use flapping wing system. Much experimental, theoretical and computational work has been performed on the understanding and prediction of the flapping airfoil aerodynamics. It is still not clearly known how to distribute the pitching angle and plunging velocity over the flapping cycle to achieve a desired mean thrust and lift, at the same time minimize the power required to flap the wings at realistic frequencies and amplitudes.

Many important features of flapping airfoil behavior are depicted by the classical linear theory. Theodorsen[1] developed compact expressions for forces and moments of a flapping airfoil under the assumption of small perturbed inviscid and incompressible flow. The flow is treated in two classes: the non-circulating flow and the circulatory flow due to wake vortices. The thrust force and the power input experienced by the flapping airfoil were given by Garrick.[2]

Ho and Chen[3] studied the unsteady wake of a plunging airfoil NACA 0012 in a low turbulence wind tunnel by a miniature multiple hot-wire probe at Reynolds number ($2.1 \times 10^4 \sim 10^5$), reduced frequency ($0 \sim 1$), and mean angle of attack 5°. Under the condition of no dynamic stall, the near wake consists of viscous part and an inviscid part. The viscous wake is the result of the merging of two boundary layers on

*Post-Doctoral Researcher. AIAA member
†Researcher.
‡Professor. Associate Fellow AIAA.
§Principal Research Scientist, AIAA Member

the airfoil, has high velocity gradient and high turbulence levels, and is limited in a very thin region. The inviscid wake is caused by the induced flow of the circulation around the plunging airfoil and is laminar and of large width.

Water-tunnel tests of the NACA 0012 airfoil oscillated sinusoidally in plunge were performed by Jone, Dohring and Platzer.[4] Excellent agreement with numerical computations from an inviscid, incompressible, unsteady panel code that utilizes a nonlinear wake model indicates that the formation and evolution of the thrusting-indicative wake structures are primarily an inviscid phenomena.

Anderson[5] and Anderson, Streitlien, Barrentt, and Triantafyllou[6] obtained visualization and force data for a plunging and pitching airfoil NACA 0012 moving in a water tank facility over a large range of amplitudes, frequencies, and phase angles. Propulsive efficiency, as high as 87% is measured experimentally under conditions of optimal wake formation. They found that agreement between the experimental data and numerical predictions of a nonlinear incompressible unsteady potential-flow method is good when either very weak or no flow separation vortices form.

Neef and Hummel[7] computed the two-dimensional airfoils and three-dimensional high aspect ratio wings by using Euler equations. Guided by the cruising flight of large birds, the reduced frequency is limited to the order of 0.1 and the pitching oscillation advances about 90° ahead of the plunging oscillation. High propulsive efficiency of the order of 90% is observed and the flow around the wing remains in the regime of attached flow.

Isogai, Shinmoto and Watanabe[8] simulated dynamic stall phenomena around a flapping NACA 0012 airfoil by a Navier-Stokes code at a freestream Mach number of 0.3 and Reynolds number of 10^5. A Baldwin and Lomax algebraic turbulence model[9] is used in the computation. They found that high propulsive efficiency occurs for the case in which the pitching oscillation advances 90° ahead of the plunging oscillation and the reduced frequency is at some optimum value, for which there appears no appreciable flow separation in spite of large-amplitude oscillations.

Tuncer, Walz and Platzer[10] using a thin-layer Navier-Stokes solver computed one case of Isogai et al.[8] with the Baldwin and Lomax turbulence model. It was noted that although the agreements between the two computations are fairly good in most conditions, large quantitative discrepancies are seen for some conditions with unknown reason.

Tuncer and Platzer[11] used a compressible Navier-Stokes solver to compute the unsteady turbulent flow fields and obtained high propulsive efficiency when the flow remains mostly attached over the airfoil oscillated in plunge and pitch.

Very recently, Young and Lai[12] used a compressible Navier-Stokes solver and an incompressible unsteady potential flow code to simulate the flow over a sinusoidally oscillating NACA 0012 airfoil. Free-stream Mach number 0.05 and 0.2 were used in their compressible Reynolds averaged Navier-Stokes flow solver. They found that the freestream Mach number has an important effect on the force predicted for both pitching and plunging oscillations. Their computed wake structures closely agree with experimental wake visualizations when the flow is assumed to be fully laminar at the chord Reynolds number 2×10^4.

Fung and Carr[13] studied the experimental data of McCroskey et al.[14] on dynamic stall for a pitching-oscillating NACA 0012 airfoil with an amplitude of 10° and mean angle of attack of 15°. They found that the critical freestream Mach number is as low as 0.2 due to the high instantaneous angle of attack in. A local supersonic flow region starts to occur over the airfoil surface.

Optimization may be performed for high propulsion efficiency, or high thrust individually or a combination of the two. Efficiency may be the more important selection in cruising flight, whereas high thrust coefficient may be more important in acceleration.

The time-accurate Euler method serves to isolate the viscosity and can determine the relative importance of inviscid elements of the controlling physics in unsteady attached flows. It is indispensable to take into account the effects of viscosity beyond the dynamic-stall boundary. However, high propulsive efficiency is often obtained for flapping airfoil when dynamic stall is delayed to large angle of attack and the efficiency drops significantly when a separation vortex forms because additional work has to be done against the suction induced by the vortex. The aim of this paper is to find a general and robust route to search for optimal motion parameters of the combined pitching and plunging oscillation under the condition of fully attached flow by an Euler method and with the help of the classical linear theory.

In the following sections, the Euler solver and the computation model are described. Appropriate dynamic stall boundary is selected based upon available experimental data and Navier-Stokes computational results in the literature. Optimum motion parameters within the dynamic stall boundary are first roughly determined

by means of the classical linear oscillating airfoil theory and then refined by the Euler computations. After studying several cases in the literature, an optimization over a large range of various motion parameters is made. The effect of mean angle of attack on the propulsive efficiency and thrust coefficient is investigated.

II. Euler Solver

It is known that the Euler solver can capture automatically the inviscid wake, i.e., the vorticity shed from the sharp trailing edge and its rolling up into vortex cores while convected downstream. Although the boundary layer together with its wake is absent in the Euler solutions, the gross dominant characteristics of the wake, i.e., the primary trailing-edge vortex configurations and their interactions with the moving body surface are reproduced as long as there are no significant boundary-layer separations.

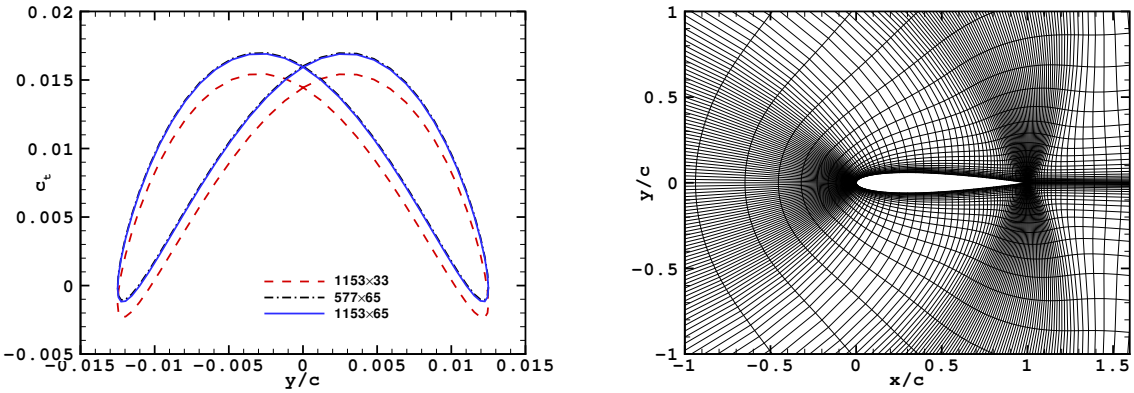

Figure 1. Numerical experiments on C-type-grid refinement (left) and close-up view of the grid, 577×65, for flapping NACA 0012 airfoil and near wake, only every other line is plotted in the figure for clarity.

The present Euler solver is based on a multi-block, multigrid, finite-volume method and parallel code for the three-dimensional, compressible steady and unsteady Euler and Navier-Stokes equations. The method uses central difference with a blend of second- and fourth-order artificial dissipation and explicit Runge-Kutta-type time marching. The coefficients of the artificial dissipation depend on the local pressure gradient. The order of magnitude of the added artificial dissipation terms is of the order of the truncation error of the basic scheme, so that the added terms have little effect on the solution in smooth parts of the flow. Near the steep gradients the artificial dissipation is activated to mimic the physical dissipation effects. Unsteady time-accurate computations are achieved by using a second-order accurate implicit scheme with dual-time stepping. The solution for each real-time step is solved by an explicit time-marching scheme in a fictitious time in which the local time stepping, residual smoothing, and multigrid techniques can be used to accelerate convergence to a steady state until the maximum residual of the continuity equation is reduced by more than 5 orders of magnitude. Computations are performed with single precision of the computing machine. The resulting code preserves symmetry.[15]

On the airfoil surface the instantaneous flow normal velocity component is set equal to the local surface normal velocity component prescribed by the oscillatory motion. The far field boundary is located at 20 chord length away from the airfoil. At the far-field inflow and outflow boundaries the flow variables are evaluated using the zero-th order Riemann invariant extrapolation. The initial condition is the airfoil starting from a position in its oscillatory motion in a free-stream flow and unique solution is obtained for any position used for the initial condition. The solver has been validated for a number of steady and unsteady cases.[16–22]

The present Euler solver was originally designed for compressible flow. It is known that the numerical solution of a compressible flow solver may not converge to the physical incompressible flow as the free-stream Mach number goes to zero. To remove this problem, a preconditioning techniques to treat the compressible-flow solver were proposed by Turkel.[23] However, in many cases, there exists small nonzero free stream Mach numbers at which the compressible code would yield good approximate low speed flows. In this paper, instead of implementing the preconditioning techniques, appropriate small free-stream Mach numbers are used to simulate the low speed flow over the flapping airfoil. The numerical experiments[20] showed that

the freestream Mach numbers can be set as low as 0.025 provided a minor anomaly in the surface pressure distribution at the trailing edge is allowed. In fact, in the low speed freestream air flow, a flapping airfoil may induce high instantaneous local Mach number due to large effective angle of attack. Therefore a compressible flow solver is needed after all. In this paper to simulate low speed flow, the freestream Mach number is set at 0.1.

The C-type grid, 577×65 moving with the flapping airfoil is used for all the computations in this paper. There are 385 grid points around the airfoil, and 97 vertical grid lines and 129 horizontal grid lines in the region downstream of the airfoil. This grid yields aerodynamic forces which are grid-independent. It is obtained by the numerical experiments as shown in Fig. 1 (left). In this figure, the computed instantaneous inviscid thrust coefficient, c_t, is plotted versus the vertical position y/c of a plunging NACA 0012 airfoil with a nondimentional plunging amplitude of 0.0125, reduced frequency of 4.0 and freestream Mach number of 0.1. c_t is most sensitive to the grid density among the various aerodynamic coefficients. A close-up view of the grid for the airfoil and its near wake is shown in Fig. 1 (right). Only every other line is plotted in the figure for clarity. The numerical experiments of time-step refinement were also performed and the solutions with a step number per cycle, $nstep = 64$ are time-step independent. In all computations in this paper the real-time unsteady solution becomes periodic after about five cycles of the oscillation.

It is known that flow bifurcation appears in pure plunge at zero mean angle of attack when the maximum instantaneous angle of attack is extremely large. Jones et al.[4] reported a deflected vortex street and a non-zero time-averaged lift for the case $k = 6.15, h = 0.12$ (or maximum effective angle of attack equal to 55.88 degrees) in water-tunnel experiments and reproduced this phenomena by a potential-flow code using different initial conditions. Lewin et al.[24] also demonstrated the flow switching by a viscous-flow code. For the cases computed in the present paper, the numerical solutions of the Euler solver are independent of the initial conditions.

III. Computational Model

A coulped pitching and plunging oscillation on NACA 0012 airfoil is considered. The plunging oscillation is defined as a vertical flapping at right angles to the direction of uniform freestream of velocity U_∞. The NACA 0012 airfoil with chord length c performs a sinusoidal plunging. The position of the airfoil is $y(t)$.

$$y(t) = y_0 \sin(\omega t). \tag{1}$$

where t is physical time, ω and y_0 are the angular frequency and the amplitude of the plunging oscillation, respectively, y is positive in the upward direction.

Nondimensional plunge amplitude is $h = y_0/c$. Reduced frequency is $k = \omega c/2U_\infty$. The instantaneous nondimensional plunging velocity is

$$\dot{y}/U_\infty = 2hk \cos(\omega t). \tag{2}$$

where a dot denotes a differentiation with respect to t. The nondimensional maximum plunging velocity, $\omega y_0/U_\infty = 2hk$. The instantaneous effective angle of attack due to pure plunging is

$$\alpha_h = \tan^{-1}(-\dot{y}/U_\infty). \tag{3}$$

where α_h is positive in the nose-up direction. The maximum effective angle of attack over a pure-plunging cycle is $\tan^{-1}(2hk)$.

The coupled pitching oscillation is defined as rotating about a point on the airfoil chord at a distance ac from the leading edge. The instantaneous angle measured clockwise from the mean chord is α.

$$\alpha = \alpha_1 sin(\omega t + \phi) \tag{4}$$

where α_1 is the amplitude of pitching oscillation, ϕ is the phase angle ahead of the plunging motion. Pitching oscillation induces not only an angle of attack effect but also a dynamic-cambering effect to the airfoil due to the angular velocity about the pitching pivot point, a.

The angle of attack amplitude ratio of the coupled pitching-plunging oscillation is denoted as λ.

$$\lambda = \alpha_1 / tan^{-1}(2hk) \tag{5}$$

The instantaneous effective angle of attack for the coupled pitching and plunging oscillation is denoted by α_e.

$$\alpha_e = \alpha_0 + \alpha + \tan^{-1}(-\dot{y}/U_\infty) \tag{6}$$

where α_0 is the mean angle of attack. The maximum effective angle of attack over a pitching-plunging-oscillation cycle, $|\alpha_e|_{max}$ is a function of α_0, α_1, h, k, and ϕ and can be evaluated by numerical method.

The importance of a phase shift near 90° can be appreciated by an example: $\alpha_0 = 0$, $\alpha_1 = 30°$, $h = 1.25$, $k = 0.27$ and $\phi = 90°$. A plot of the instantaneous angle of attack due to the pitching α, the plunging α_h and the coupled pitching-plunging α_e versus ωt is shown in Fig. 2 for the case $\alpha_0 = 0$, $\alpha_1 = 30°$, $h = 1.25$, $k = 0.27$ and $\phi = 90°$. The maximum angle of attack of the pure pitching oscillation is 30°. The maximum effective angle of attack of the pure plunging oscillation is 34.02°. The maximum effective angle of attack of the coupled oscillation $|\alpha_e|_{max} = 4.37°$ which is about the difference of the maximum angles of attack of the pitching and the plunging because the pitching leads the plunging by the phase angle, $\phi = 90°$.

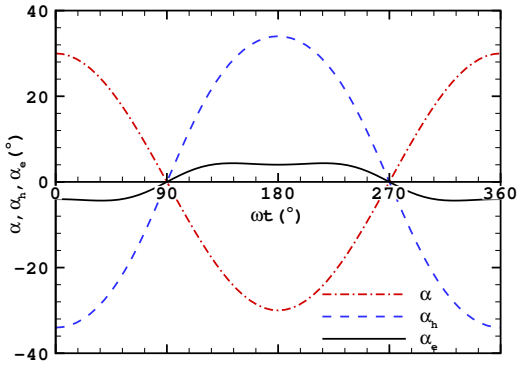

Figure 2. Instantaneous angles of attack due to oscillation of pure pitching, pure plunging and coupled pitching-plunging oscillation, α, α_h, and α_e, respectively, versus ωt, $\alpha_0 = 0$, $\alpha_1 = 30°$, $h = 1.25$, $k = 0.27$ and $\phi = 90°$.

The instantaneous lift and (inviscid) thrust coefficients are c_l and c_t, respectively. The instantaneous pitching moment coefficient around the pitching-pivot-point is c_m (positive in the nose-up sense). The instantaneous input power coefficient is $c_{ip} = -(c_l\dot{y} + c_m c\dot{\alpha})/U_\infty$.

The time-averaged lift coefficient, pitching moment coefficient, thrust coefficient and input power coefficient over an oscillation period are C_L, C_M, C_T and C_P, respectively. The propulsive efficiency $\eta = C_T/C_P$.

Under the assumption of no dynamic stall, the Euler method can predict the unsteady pressure distribution and thereby provide the instantaneous and cycle-averaged lift, pitching moment, power input, and inviscid drag over the plunging airfoil, but not the viscous profile drag. The viscous profile drag can be modeled using an interactive inviscid flow and boundary layer calculation, or approximately by quasi-steady drag polar correlations of the airfoil. For example, the quasi-steady skin friction of the two sides of a smooth flat plate[25] C_F is subtracted from the inviscid thrust coefficient C_T computed from the Euler method as an approximate modeling of the viscous effects. For laminar flow, $C_F = 2 \times 1.328/Re^{1/2}$. For turbulent flow, $C_F = 2 \times 0.072/Re^{1/5}$.

IV. Dynamic-Stall-Onset Angle of Attack

Experiments and Navier-Stokes computations have shown that the primary parameter that determines the onset of separation is the maximum effective angle of attack in a whole cycle of oscillation, $|\alpha_e|_{max}$. The dynamic-stall-onset angle of attack is denoted by α_{DS}. When $|\alpha_e|_{max} < \alpha_{DS}$, the flow is fully attached. α_{DS} depends largely on the mean angle of attack, amplitude of plunging and pitching oscillation, reduced frequency, free stream Mach number and Reynolds number, airfoil shape and type of motion. The NACA 0012 airfoil is considered in this paper.

From the experimental data of Ref. 14 for pure pitching oscillation of NACA 0012 airfoil over a range of reduced frequency ($k = 0.1 \sim 0.2$), mean angle of attack, and amplitude of oscillation, the dynamic-stall-onset angle of attack, $\alpha_{DS} \approx 14^\circ$ at $M_\infty \approx 0.3$ and Reynolds number based on chord $Re \approx 4 \times 10^6$. (See Fig. 2 of Ref. 26.)

The pure plunging oscillation of NACA 0012 airfoil at $M_\infty = 0.3$ and $Re = 10^6$ for fully turbulent flow were computed by Tuncer et al.[10] using a thin-layer Navier-Stokes solver with the Baldwin-Lomax turbulence model. Their figures 1 and 2 plotted the curve C_T versus h at constant k. The dynamic-stall onset boundary can be defined as the point where the slope of the curve starts to decrease with the increase of h at constant k, which indicates that a significant boundary-layer separation occurs. With this criterion a series of nonseparated and separated solutions approaching the dynamic stall onset boundary from opposite sides of the boundary are taken. Fig. 3 (left) presents the maximum effective angle of attack $|\alpha_e|_{max}$ versus the reduced frequency k for the separated and nonseparated solutions close to the dynamic-stall boundary. The dynamic-stall-onset angle of attack, α_{DS}, increases from 16.7° to 24.2° when k increases from 0.125 to 1.5.

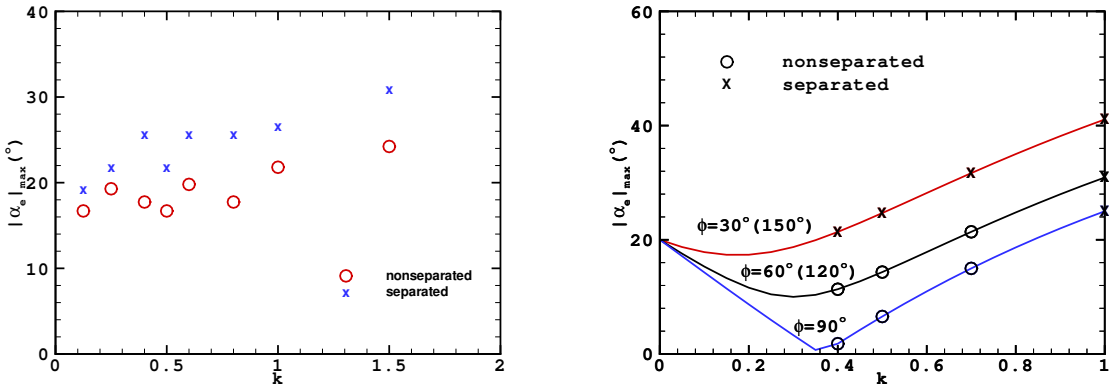

Figure 3. Maximum effective angle of attack $|\alpha_e|_{max}$ of separated and nonseparated Navier-Stokes solutions obtained by Tuncer et al.[10] for pure plunging oscillation at $Re = 10^6$ (left) and Isogai et al.[8] for pitching-plunging oscillation at $Re = 10^5$ versus reduced frequency k, NACA 0012 airfoil turbulent flow, $M_\infty = 0.3$.

The coupled pitching-plunging oscillation of the NACA 0012 airfoil at $h = 0.5$, $\alpha_0 = 0$, $\alpha_1 = 20^\circ$, $M_\infty = 0.3$ and $Re = 10^5$ in fully turbulent flow was computed by Isogai et al.[8] using a Navier-Stokes solver with the Baldwin-Lomax turbulence model. The maximum effective angle of attack versus reduced frequency k and phase angle ϕ for various separated and nonseparated solutions are presented in Fig. 3 (right) which is reproduced from Fig. 8 of Isogai et al. It is seen that the dynamic-stall-onset angle of attack $\alpha_{DS} \approx 20^\circ$ for $k = 0.4 \sim 1.0$. From Fig. 16 of Isogai et al., for another case, $h = 1.0$, $\alpha_0 = 0$ and $\alpha_1 = 10^\circ$, $\alpha_{DS} = 14^\circ \sim 20^\circ$ for $k = 0.15 \sim 0.5$.

From the experimental data of Ref. 14, the static-stall angle of attack for the NACA 0012 airfoil is 13.7° at the same M_∞ and Re of the pitching test. It is seen that the dynamic-stall angle of attack for pure pitching oscillation is nearly equal to the static-stall angle of attack, while that for pure plunging is significantly greater than the static-stall angle of attack. This distinction is caused by the difference in the type of the two motions. For pure plunging, the effective angle of attack results from the translational velocity of the airfoil, while for pure pitching, besides a uniformly distributed angle of attack along the airfoil chord there exists a nonuniformly distributed angle of attack along the airfoil chord. Due to the rotational velocity of the airfoil $\dot{\alpha}$, a distribution of varying angle of attack along the airfoil chord is formed in addition to the uniform angle of attack. When the airfoil starts to rotate counter-clockwise from its maximum angle of attack, $\dot{\alpha} < 0$, which produces an increment to the local angle of attack at the airfoil leading edge and tends to activate a dynamic stall. Moreover, in the mean time the rotational acceleration $\ddot{\alpha} < 0$ which produces a pure couple in the clockwise direction (See Section 13.4 of Fung[27]) and furthers the tendency towards dynamic stall.

Neef et al.[7] in computing the coupled pitching-plunging oscillation of NACA 0012 airfoil at $M_\infty = 0.3$ with $k \approx 0.1$ by an Euler solver suggested keeping the maximum effective angle of attack below $12^\circ \sim 15^\circ$

in order to ensure attached flow.

For coupled pitching-plunging oscillation of NACA 0012 airfoil in incompressible flow, Anderson et al.[6] observed from visualization data at $Re = 1100$ that $\alpha_{DS} \approx 20^\circ$ for $h = 1.0$, $\alpha_0 = 0$, $\alpha_1 = 0 \sim 15^\circ$, $\phi = 90^\circ$ and $k = 0.16$. (See Fig. 17 and Table 1 of Ref. 6.)

Based on the above experimental data and Navier-Stokes computations, in the present computation of coupled pitching-plunging NACA 0012 airfoil at a low Mach number 0.1 by the Euler solver, $|\alpha_e|_{max} \leq (15^\circ \sim 20^\circ)$ is required in order to ensure attached flow throughout the whole flapping cycle.

V. Optimization Computations of Specific Cases, $\alpha_0 = 0$

Optimization computations are made for several specific cases studied in the literature. The classical linear theory is used to provide a prelimilary optimization. The Euler method is first validated by the known computational and experimental results of nonseparated or lightly separated flows, and then used to refine the optimization. Four cases are considered, namely two cases of Isogai et al.,[8] a case of Neef et al.[7] and a case of Anderson et al.[6] In all the cases, h, α_1, and a are given and $\alpha_0 = 0$. The optimization computation procedures are as follows.

1. Calculate the maximum effective angle of attack, $|\alpha_e|_{max}$, for given h and α_1 and plot as function of k and ϕ;

2. Plot the contours of C_T and η on the plane of ϕ and k by the linear theory for given h, α_1 and a, and plot the dynamic-stall boundary, $|\alpha_e|_{max} = 15^\circ$ (or 20°) on the plane (ϕ, k) for the given h, and α_1;

3. Select optimum values of k and ϕ within the dynamic-stall boundary from the C_T and η contour-maps of the linear theory and recompute C_T and η by the Euler solver;

4. Search for the optimum in the vicinity of the selected k and ϕ by optimization techniques with the Euler solver.

A. $h = 0.5$, $\alpha_1 = 20^\circ$, $a = 1/2$, $M_\infty = 0.3$

Isogai, Shinmoto and Watanabe[8] simulated dynamic stall phenomena around a flapping NACA 0012 airfoil by a Navier-Stokes code at $M_\infty = 0.3$ and $Re = 10^5$ using a Baldwin and Lomax algebraic turbulence model.[9] Their case A: $h = 0.5$, $\alpha_1 = 20^\circ$ and $a = 1/2$ is revisited here.

The maximum effective angle of attack, $|\alpha_e|_{max}$, as a function of k and ϕ, is calculated for $h = 0.5$, $\alpha_1 = 20^\circ$ and presented in Fig. 4 (left). Based on the Navier-Stokes computations,[8] the dynamic-stall boundary is determined to be $|\alpha_e|_{max} = 20^\circ$ for $k = 0.4 \sim 1.0$.

Fig. 4 (right) gives the contours of the time-averaged thrust coefficient, C_T and the propulsive efficiency, η versus k and ϕ obtained from the linear theory for $h = 0.5$, $\alpha_1 = 20^\circ$, $a = 1/2$. The scale of the angle of attack amplitude ratio, λ, corresponding to k is marked. Two dynamic-stall boundaries, $|\alpha_e|_{max} = 15^\circ$ and 20° are also plotted in the figure. To avoid dynamic-stall, the range of ϕ is limited as $(0, 180^\circ)$. The contours of $C_T = constant$ are open and the value of C_T increases with the increase of k. $C_T < 0$ is not shown in the figure. The contours of $\eta = constant$ become closed when η is large. The location of the peak value of η is biased to that of lower C_T and near $\phi = 90^\circ$. In general, with the increase of reduced frequency the thrust coefficient increases but the efficiency decreases. As the flow becomes more and more unsteady with increasing reduced frequency, a large amount of vorticity shed from the trailing edge, the thrust increases but the efficiency decreases.

Table 1 Comparison of the present computations with the nonseparated Navier-Stokes solutions[8] and two optimum cases obtained by the Euler method (last 2 rows) for Case A.

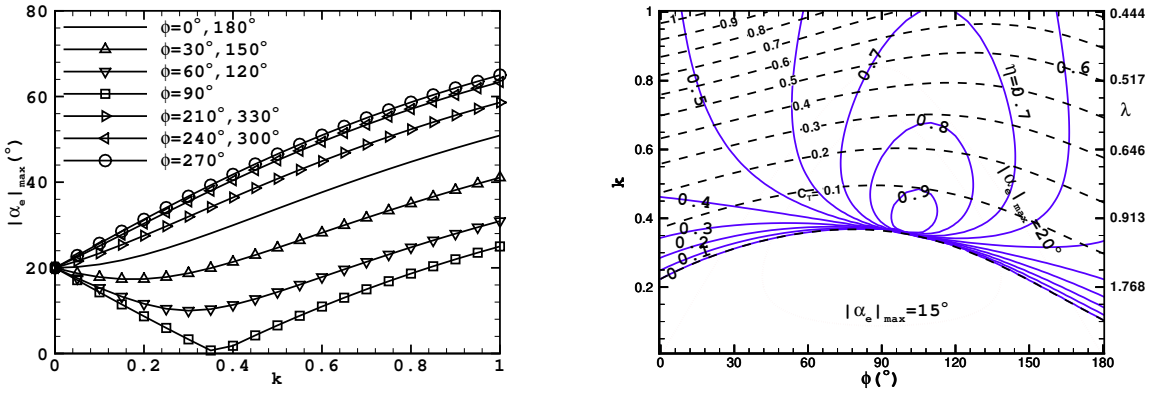

Figure 4. Maximum effective angle of attack $|\alpha_e|_{max}$ for $h = 0.5$, $\alpha_1 = 20°$ (left), and contours of time-averaged thrust coefficient C_T and propulsive efficiency η of NACA 0012 airfoil 0012 on the plane (ϕ, k) computed by linear theory, $h = 0.5$, $\alpha_1 = 20°$, $a = 1/2$.

			Euler		Navier-Stokes[8]	
k	$\phi(°)$	$\lvert\alpha_e\rvert_{max}(°)$	C_T	$\eta(\%)$	C_T	$\eta(\%)$
0.4	90	1.81	0.00738	61.5	0.0637	34.1
0.4	60	11.3	0.0540	81.4	0.0301	49.6
0.5	90	6.57	0.0778	79.9	0.0768	72.3
0.5	60	14.3	0.123	83.5	0.0975	64.4
0.5	120	14.3	0.0681	41.5	0.0709	40.5
0.7	90	15.0	0.266	70.9	0.271	65.2
0.7	120	21.4	0.277	50.3	0.286	50.4
0.49	115	12.3	0.110	86.7	N/A	N/A
0.83	90	19.7	0.452	64.7	N/A	N/A

In the paper of Isogai et al.,[8] the thrust is obtained from integrating their computed pressure distribution and, thus, it is the inviscid part of the thrust and can be compared directly with the Euler result. However, their definition for the thrust coefficient is different from that in this paper. To facilitate a direct comparison, the thrust coefficients given by Isogai et al. are converted to fit the present definition. Table 1 presents the comparison of the time-averaged pressure thrust coefficient and the propulsive efficiency computed by the Euler solver with the nonseparated solutions of Isogai et al.[8] Fig. 5 plots the Euler-computed time-averaged pressure thrust coefficient against ϕ at $k = 0.4$, 0.5 and 0.7 (left) and propulsive efficiency against ϕ at $k = 0.5$ (The cases of $k = 0.4$ and 0.7 are similar and not shown for clarity.) from Table 1 and gives the results of the linear theory for comparison. The agreements between the two computations are fairly good for C_T. But the large quantitative discrepancies in η require further investigation. The linear theory roughly agrees with the computations in this case.

With the aid of the linear theoretical results, two optimum cases are found within the dynamic-stall boundary and confirmed by the Euler solver. The case at $k = 0.49$ and $\phi = 115°$ yields $\eta = 0.867$ and $C_T = 0.110$ which has the highest propulsive efficiency and a comparable thrust coefficient. Another case at $k = 0.83$ and $\phi = 90°$ yields the highest thrust coefficient, $C_T = 0.452$ and $\eta = 0.647$. They are listed in the last two rows of Table 1.

B. $h = 1.0$, $\alpha_1 = 10°$, $a = 1/2$, $M_\infty = 0.3$

The case B of Isogai et al.:[8] $h = 1.0$, $\alpha_1 = 10°$ and $a = 1/2$ is revisited here. Fig. 6 presents the maximum effective angle of attack versus k at constant ϕ for $h = 1.0$ and $\alpha_1 = 10°$ (left) and the contours of the time-averaged thrust coefficient and the propulsive efficiency over flapping cycle of an NACA 0012 airfoil on the plane of ϕ and k computed by the linear theory for $h = 1.0$, $\alpha_1 = 10°$ and $a = 1/2$. Based on

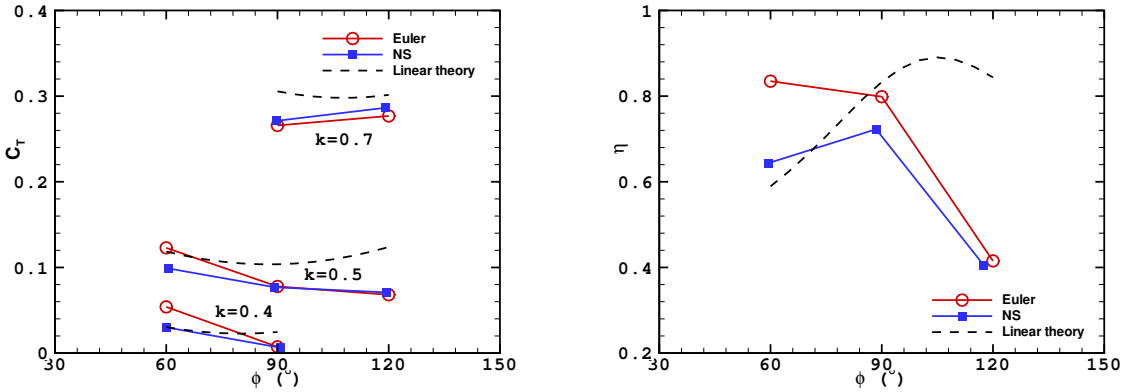

Figure 5. Euler-computed time-averaged pressure thrust coefficient vs. ϕ at $k = 0.4$, 0.5 and 0.7 (left) and propulsive efficiency vs. ϕ at $k = 0.5$ compared with Navier-Stokes solutions[8] and linear theory, $h = 0.5$, $\alpha_1 = 20°$, $a = 1/2$.

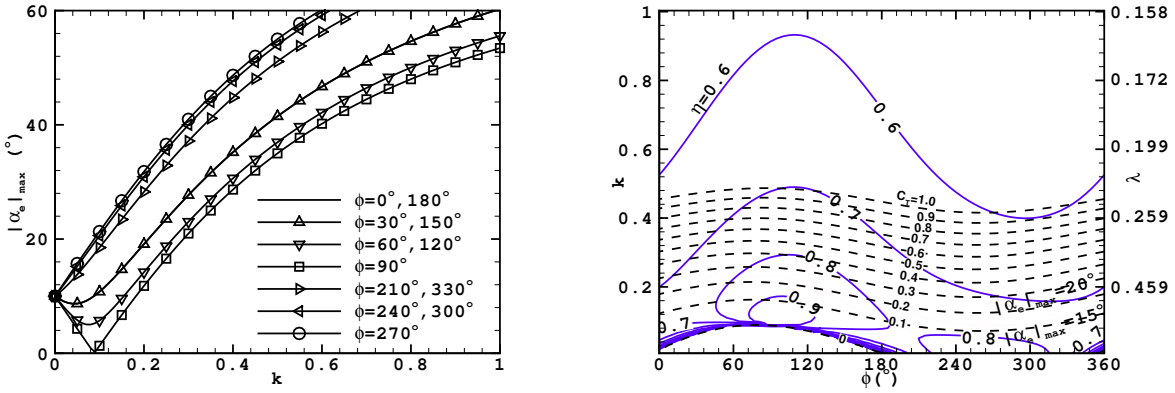

Figure 6. Maximum effective angle of attack $|\alpha_e|_{max}$ for $h = 1.0$ and $\alpha_1 = 10°$ (left) and contours of time-averaged thrust coefficient C_T and propulsive efficiency η of NACA 0012 airfoil 0012 in the plane (ϕ, k) computed by linear theory for $h = 1.0$, $\alpha_1 = 10°$ and $a = 1/2$.

the Navier-Stokes computations,[8] the dynamic-stall boundary is determined to be $|\alpha_e|_{max} = 14^\circ \sim 20^\circ$ for $k = 0.15 \sim 0.5$. Two dynamic-stall boundaries, $|\alpha_e|_{max} = 15^\circ$ and 20° are plotted in the right figure. In this case, they are no longer closed and the entire range of ϕ $(0, 360^\circ)$ is considered. The behavior of the contours of C_T and η are similar to that of Fig. 4 except there appears a secondary peak of η. The primary peak occurs at about $\phi = 90^\circ$. The seconary peak occurs near $\phi = 270^\circ$.

This case was also computed by a Navier-Stokes code by Tuncer et al.[10] at the same M_∞ and Re using the same turbulence model. The two Navier-Stokes computations were compared directly each other in their papers. It is presumed that the thrust given by Tuncer et al. was also obtained from pressure integration as Isogai et al. did. To compare them with the Euler solutions, their thrust coefficients are also converted into the present definition. Table 2 presents the comparison of the time-averaged pressure thrust coefficient and the propulsive efficiency computed by the Euler solver with the nonseparated Navier-Stokes solutions of Isogai et al.[8] and Tuncer et al.[10] Fig. 7 plots the Euler-computed time-averaged pressure thrust coefficient and propulsive efficiency against ϕ at $k = 0.15$ and gives the results of the linear theory for comparison. The Euler computations and the two Navier-Stokes computations are in qualitative agreement. The Euler results agree better with those of Tuncer et al. than with those of Isogai et al. The difference in η between the Euler solutions and the Navier-Stokes solutions of Tuncer et al. is even smaller than the difference between the two Navier-Stokes solutions. Again, the linear theory roughly agrees with the computations in this case.

With the aid of the linear theoretical results, a thrust-optimum case is found within the dynamic-stall boundary and confirmed by the Euler solver. The case at $k = 0.28$ and $\phi = 90^\circ$ yields $C_T = 0.359$ and $\eta = 0.711$ and is listed in the last row of Table 2.

Table 2 Comparison of the present computations with the nonseparated Navier-Stokes solutions and a thrust-optimized case obtained by the Euler method (last row) for pitching-plunging NACA 0012 airfoil $h = 1.0$, $\alpha_1 = 10^\circ$, $a = 1/2$, $M_\infty = 0.3$.

			Euler		Ref. 8		Ref. 10	
k	$\phi(^\circ)$	$\lvert\alpha_e\rvert_{max}(^\circ)$	C_T	$\eta(\%)$	C_T	$\eta(\%)$	C_T	$\eta(\%)$
0.15	90	6.70	0.0873	89.8	0.0646	79.1	0.0735	88.5
0.15	60	9.58	0.116	88.1	0.0883	77.2	0.102	81.1
0.15	120	9.58	0.0829	79.9	0.0569	68.1	0.0565	78.1
0.28	90	19.2	0.359	71.1	N/A	N/A	N/A	N/A

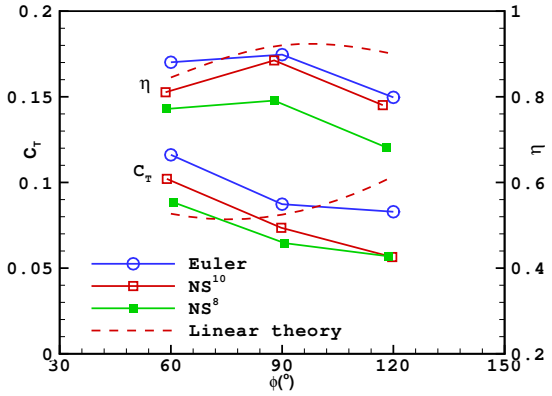

Figure 7. Euler-computed time-averaged pressure thrust coefficient and propulsive efficiency vs. ϕ at $k = 0.15$ compared with Navier-Stokes solutions of Refs. 8 and 10 and linear theory, $h = 1.0$, $\alpha_1 = 10^\circ$, $a = 1/2$.

C. $h = 0.75$, $\alpha_1 = 30^\circ$, $a = 1/3$, $M_\infty = 0.1$

Anderson et al.[6] obtained a high propulsive efficiency case: $h = 0.75$, $\alpha_1 = 30^\circ$, $a = 1/3$, $k = 0.67$, and $\phi = 75^\circ$, through optimal wake formation in water-tank experiments. Their visualization results showed

that conditions of high efficiency are associated with the formation of a moderately strong leading-edge vortex per half cycle at $Re = 1100$. The corresponding force measurements gave $\eta = 0.87$ and $C_T = 0.52$ at $Re = 4 \times 10^4$. (See Table 3, Case 2 of Ref.6.) Accordingly, the case $h = 0.75$, $\alpha_1 = 30°$, $a = 1/3$, and $M_\infty = 0.1$ is studied here.

Fig. 8 gives the maximum effective angle of attack versus k at constant ϕ for $h = 0.75$, and $\alpha_1 = 30°$ (left) and the contours of the time-averaged mean thrust coefficient and the propulsive efficiency over a flapping cycle of an NACA 0012 airfoil in the plane of ϕ and k computed by the linear theory. From Fig. 8 (left), the maximum effective angle of attack for $k = 0.67$, and $\phi = 75°$, $|\alpha_e|_{max} = 20.4°$ is slightly greater than the dynamic-stall angle of attack, $\alpha_{DS} \approx 20°$. Thus, the high propulsive efficiency case obtained by Anderson et al. is attributed to the moderate separation observed.

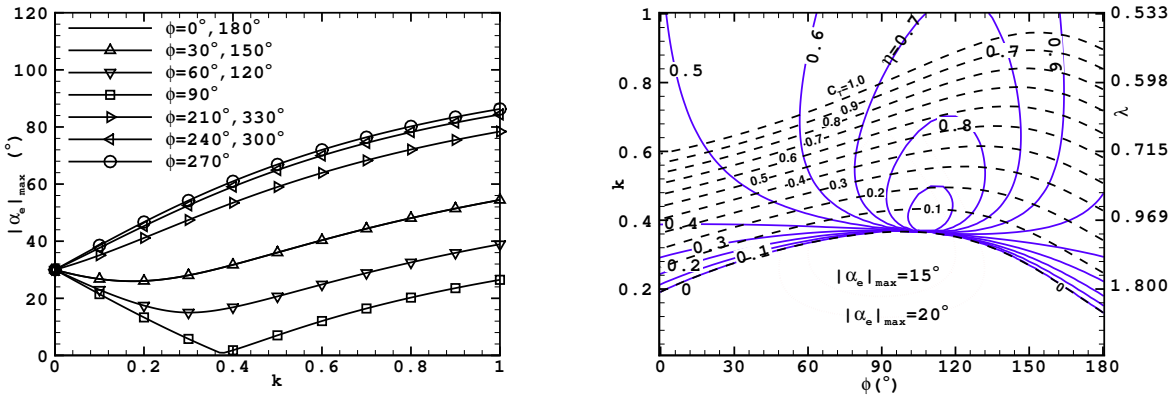

Figure 8. Maximum effective angle of attack $|\alpha_e|_{max}$ for $h = 0.75$ and $\alpha_1 = 30°$ (left) and contours of time-averaged thrust coefficient C_T and propulsive efficiency η of NACA 0012 airfoil on the plane (ϕ, k) computed by linear theory, $h = 0.75$, $\alpha_1 = 30°$, $a = 1/3$.

Table 3 Comparison of Euler computations with experimental data[6] for pitching-plunging NACA 0012 airfoil and a thrust-optimized case obtained by the Euler method (2nd row) for case C.

			Euler(Inviscid)		Euler(Friction-corrected)		Ref.6	
k	$\phi(°)$	$\|\alpha_e\|_{max}(°)$	C_T	$\eta(\%)$	C_T	$\eta(\%)$	C_T	$\eta(\%)$
0.67	75	20.4	0.491	78.6	0.478	76.5	0.52	87
0.78	90	19.5	0.863	64.5	0.850	63.5	N/A	N/A

Since the case of Anderson et al. is located outside the attached-flow region defined by $|\alpha_e|_{max} = 20°$, it cannot be simulated by the Euler method. However, for the purpose of showing the effects of the observed leading-edge separation on the thrust and efficiency, the case of Anderson et al. is computed by the Euler solver. To compare the Euler solutions with the force measurements at $Re = 4 \times 10^4$, a friction coefficient, $C_F = 0.01328$ is subtracted from the inviscid thrust coefficient where a fully laminar flow is assumed. Table 3 presents the comparison of the time-averaged thrust coefficient and the propulsive efficiency computed by the Euler solver and the viscous-corrected ones with the experimental data.[6] Indeed, the moderately strong leading-edge vortex visualized in the experiments[6] contributes to the high efficiency measured.

A neighboring point but within the dynamic-stall boundary, $k = 0.78$ and $\phi = 90°$ is selected from Fig. 8 for higher thrust and is confirmed by the Euler solver as shown in the second row of Table 3. The high time-averaged thrust case computed by the present method is: $k = 0.78$ and $\phi = 90°$ and the inviscid thrust coefficient is 0.85 with the propulsive efficiency of 65%.

D. $h = 1.0$, $\alpha_1 = 4°$, $a = 1/4$, $\phi = 90°$, $M_\infty = 0.3$

Neef et al.[7] computed the case: $h = 1.0$, $\alpha_1 = 4°$, $a = 1/4$, $k = 0.1$, $\phi = 90°$, $M_\infty = 0.3$ for a flapping NACA 0012 airfoil High propulsive efficiency of 0.89 is observed with an inviscid thrust coefficient about 0.048(See

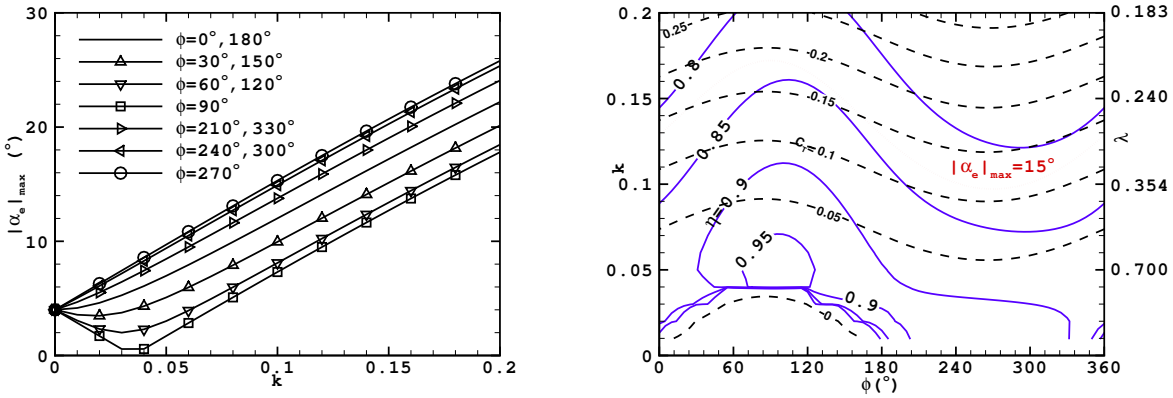

Figure 9. Maximum effective angle of attack $|\alpha_e|_{max}$ for $h = 1.0$, $\alpha_1 = 4°$ (left) and contours of time-averaged thrust coefficient C_T and propulsive efficiency η of NACA 0012 airfoil 0012 on the plane (ϕ, k) computed by linear theory, $h = 1.0$, $\alpha_1 = 4°$, $a = 1/4$.

Fig. 6 of Neef et al.). They used a coarse grid 160×32 of O-topology, whereas the present paper uses the grid 577×65 of C-topology.

Fig. 9 gives the maximum effective angle of attack versus k and ϕ (left) and the contours of the time-averaged thrust coefficient and the propulsive efficiency over a flapping cycle computed by the linear theory. The dynamic-stall boundary, $|\alpha_e|_{max} = 15°$ is plotted in the figure.

Table 4 presents the comparison of the time-averaged thrust coefficient and the propulsive efficiency computed by the present Euler solver with the Euler solutions of Neef et al.[7] The agreement between the two efficiencies is good, but a discrepancy occurs for the thrust coefficients which may be caused by the large grid-density difference of the grids used in the two computations. A thrust-optimized case at $k = 0.172$ and $\phi = 90°$ is chosen from Fig. 9 and confirmed by the Euler solver as shown in the second row of Table 4. The high inviscid thrust coefficient is 0.20 with a propulsive efficiency of 81%.

Table 4 Comparison of the present computations with the Euler solution of Neef et al.[7] and a thrust-optimized case obtained by the Euler method (2nd row) for Case D.

		Present computation		Ref.7	
k	$\|\alpha_e\|_{max}(°)$	C_T	$\eta(\%)$	C_T	$\eta(\%)$
0.1	7.31	0.0681	89.5	0.048	89
0.172	15.0	0.197	80.5	N/A	N/A

VI. Generalized Optimization, $\alpha_0 = 0$, $M_\infty = 0.1$

A generalized optimization is made in a range of the three parameters: h, α_0 and a. Each parameter takes three different values, and, in total, 27 different combinations are formed. $h = 0.75$, 1.0, and 1.25. $\alpha_1 = 10°$, 20°, and 30°. $a = 1/4$, 1/3, and 1/2. The maximum effective angle of attack is always kept not in excess of 15°. Following the optimization procedures listed in the beginning of the last section, 18 sets of optimal parameters are selected from the 27 contour-maps of C_T and η from the linear theory. Euler computations are made at $M_\infty = 0.1$.

One of the 18 cases is chosen for further optimization computations by the Euler solver. The case is:

$h = 1.25$, $\alpha_1 = 20°$, $a = 1/3$, $k = 0.28$, and $\phi = 90°$.

By means of a conventional optimization technique, using a 289×33 grid for search computations and using a fine 577×65 grid for the final results, a high propulsive efficiency of 0.90 with the inviscid thrust coefficient of 0.236 is obtained at the case:

$h = 1.25$, $\alpha_1 = 20°$, $a = 1/3$, $k = 0.22$, and $\phi = 68.5°$.

The remaining 17 cases yield directly five optimal cases. They all have moderately high thrust and efficiency. Table 5 presents all the six optimum cases obtained in this section and includes the high thrust

case from Table 3, where the first row has the highest efficiency, the second row has the highest inviscid thrust coefficient, and the rest rows have moderately high efficiency and thrust.

Table 5 Results of optimization computations by the present Euler method with the aid of the linear theory for a pitching-plunging NACA 0012 airfoil $\alpha_0 = 0$ and $M_\infty = 0.1$.

h	$\alpha_1(^\circ)$	a	k	$\phi(^\circ)$	$\lvert\alpha_e\rvert_{max}(^\circ)$	C_T	$\eta(\%)$
1.25	20	1/3	0.22	68.5	13.3	0.236	90.3
0.75	30	1/3	0.78	90	19.5	0.863	64.5
0.75	30	1/3	0.65	92	14.7	0.790	67.1
1.25	30	1/3	0.4	90	15.0	0.651	79.4
1.25	30	1/2	0.4	90	15.0	0.655	81.2
1.25	30	1/3	0.37	90	12.8	0.504	81.5
1.25	30	1/3	0.32	90	8.75	0.288	84.9

From the Euler solutions computed in this paper, the highest propulsive efficiency is 90% with a time-averaged thrust coefficient of 0.24, and the highest thrust coefficient is 0.86 with a propulsive efficiency of 65%. Higher efficieny occurs at lower reduced frequency and higher thrust occurs at higher frequency. The optimal phase angle of pitching ahead of plunging is within about 70° and 90°.

VII. Effects of Mean Angle of Attack

So far the optimizations are considered under the condition of zero mean angle of attack. The effects of the mean angle of attack on optimization are investigated in this section. Euler computations are made for the case: $h = 1.25$, $\alpha_1 = 30^\circ$, $a = 1/2$, $k = 0.27$, $\phi = 90^\circ$, and $\alpha_0 = 0 \sim 10^\circ$. $|\alpha_e|_{max} \leq 14.4^\circ$. The computation grid is 577×65 and $M\infty = 0.1$.

Fig. 10 presents the time-averaged mean lift coefficient, pitching moment coefficient (left), thrust coefficient and propulsive efficiency versus mean angle of attack for a pitching-plunging NACA 0012 airfoil computed by the Euler solver and compared with the linear theory.

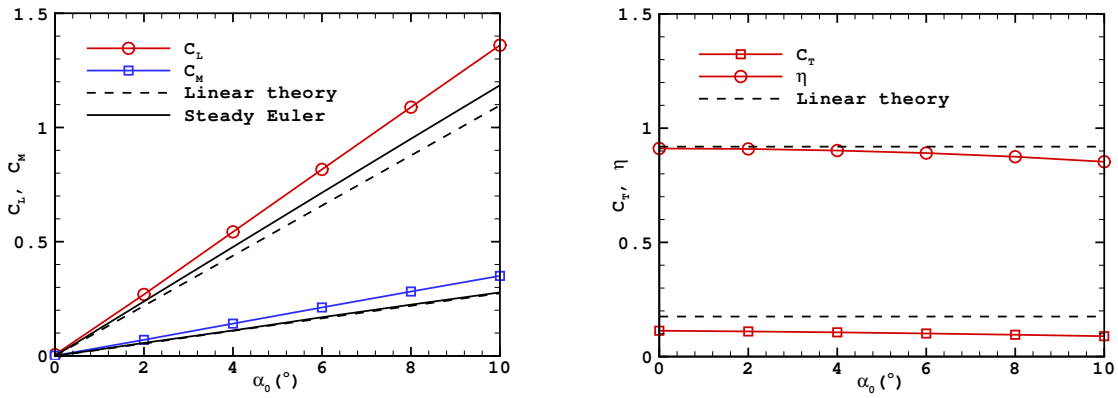

Figure 10. Time-averaged mean lift coefficient C_L, pitching moment coefficient C_M (left), thrust coefficient C_T and propulsive efficiency η versus mean angle of attack α_0 for pitching-plunging airfoil NACA 0012 computed by Euler solver and compared with linear theory, $h = 1.25$, $\alpha_1 = 30^\circ$, $a = 1/2$, $k = 0.27$, $\phi = 90^\circ$, $M\infty = 0.1$. Also, C_L and C_M versus α_0 for steady flow computed by Euler solver.

The time-averaged thrust and efficiency are almost independent of the mean angle of attack and, therefore, independent of the generation of a mean lift. This is exactly true in the linear theory. However, there are slight decreases of thrust and efficiency observed in the Euler solutions with the increase of mean angle of attack. This is a nonlinear effect captured by the Euler equations. On the other hand, the mean lift coefficient versus the mean angle of attack remains linear. The slope of the curve C_L versus α_0 computed by the Euler method becomes $1.53(2\pi)$, whereas the linear theory value is 2π. The steady-flow values computed

by the Euler method with the same grid are also shown in Fig. 10 (left), and the lift slope is $1.09(2\pi)$. Thus, the time-averaged mean lift is increased due to the flow unsteadiness. The time-averaged pitching moment is affected by the unsteady flow similarly. Therefore, the flow unsteadiness has appreciable effects on the time-averaged mean aerodynamic force and moment. The Euler solutions computed by Neef et al.[7] for a case $h = 1.0$, $\alpha_1 = 4°$, $a = 1/4$, $k = 0.1$, $\phi = 90°$, and $M_\infty = 0.3$ using a 320×64 grid, yield $dC_L/d\alpha_0 = 1.18(2\pi)$ and also a slight decrease of thrust with the increase of α_0 was observed.

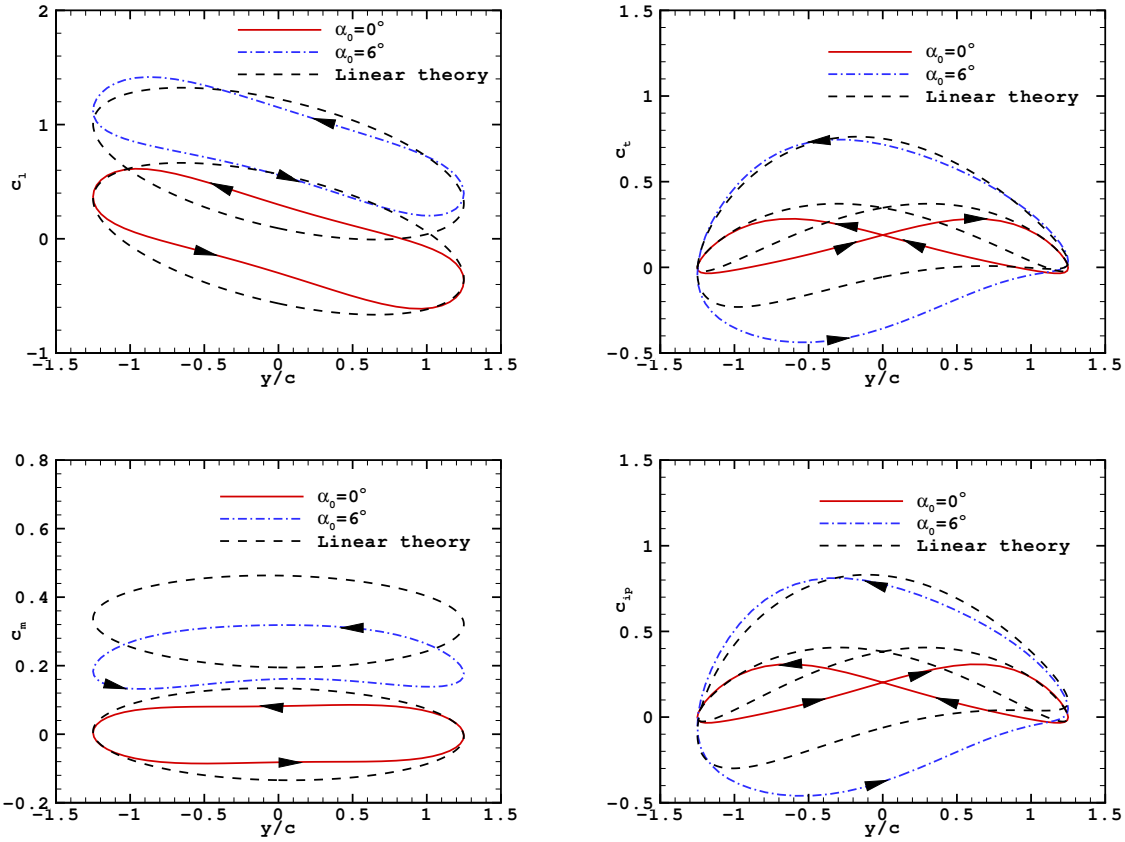

Figure 11. Instantaneous lift coefficient c_l, pitching moment coefficient c_m (left), thrust coefficient c_t and input power coefficient c_{ip} versus y/c for pitching-plunging NACA 0012 airfoil computed by Euler solver and compared with linear theory, $h = 1.25$, $\alpha_1 = 30°$, $a = 1/2$, $k = 0.27$, $\phi = 90°$, $\alpha_0 = 0$ and $6°$, $M\infty = 0.1$.

Fig. 11 presents the instantaneous lift coefficient, pitching moment coefficient (left), thrust coefficient and input power coefficient versus y/c for a pitching-plunging NACA 0012 airfoil computed by the Euler solver and compared with the linear theory for $\alpha_0 = 0$ and $6°$. The computed loops of the aerodynamic coefficients clearly demonstrate the hysteretic property existing between the up-stroke and down-stroke motion. The lift and the pitching moment are higher during down stroke than during up stroke. The effects of mean angle of attack on c_l and c_m versus y/c are a vertical translation with minor deformations in the Euler solutions. c_l and c_m are periodic functions of the same frequency as the airfoil motion. The effects on the instantaneous thrust and input power, however, are significant. If the mean angle of attack α_0 is zero, the instantaneous thrust and input power during the down stroke and the upstroke are symmetrical, and are periodic functions of the double frequency of the airfoil motion. The thrust and input power are lower during the first half of up stroke than during the second half of down stroke and become higher during the second half of up stroke than during the first half of down stroke. The scenario changes entirely when the mean angle of attack is not zero. The original two loops per cycle for c_t and c_{ip} become one loop per cycle and their frequency becomes the same as the airfoil motion. Higher thrust and input power occur during down stroke than during up stroke, and even drag and output power instead of thrust and input power can be found during the upstroke. In the linear theory, c_t and c_{ip} are quadratic functions of the angles of attack and the interactions between

the mean angle of attack and the oscillating angle of attack are displayed qualitatively.

Because the effects of the mean angle of attack on the time-averaged thrust coefficient and the propulsive efficiency are small, the optimization results obtained in the previous section are valid for non-zero mean angle of attack.

VIII. Conclusions

The time-averaged thrust coefficient of a coupled pitching-plunging NACA 0012 airfoil computed by the Euler solver agree fairly well with those obtained by pressure integration from nonseparated Navier-Stokes solutions in the literature. From available experimental data and Navier-Stokes computational results, the dynamic-stall boundary is set as the maximum effective angle of attack equals to $15 \sim 20°$. Within this boundary, the Euler method can be used to optimize the motion parameters for high thrust and/or high propulsive efficiency.

There are altogether five independent motion parameters for a coupled sinusoidal pitching-plunging airfoil at zero mean angle of attack. Given three parameters, the classical linear oscillation airfoil theory is implemented to plot the contour-map of mean thrust coefficient and propulsive efficiency in the plane of the remaining two parameters. The dynamic-stall boundary is also plotted in the plane. Optimum case for high efficiency and/or thrust is first obtained from the contour-map within the dynamic-stall boundary. Guided by the preliminary choice from the contour-map, a search for the optimum case can be readily done with the Euler computation and by conventional optimization techniques.

In principle, the form of the five independent parameters is not unique and among the five independent variables the three may be selected arbitrarily. As an example, the pitching-pivot position, the pitching amplitude, and the plunging amplitude are given and the reduced frequency and phase angle between pitching and plunging are the two variables to be optimized in this paper. The pitching-pivot position has minor effect on the optimization. The optimal phase angle of pitching ahead of plunging is about 70° to 90°. The highest propulsive efficiency and the highest thrust coefficient do not occur at the same frequency. Higher efficiency usually occurs at lower reduced frequency, and higher thrust occurs at higher reduced frequency.

The mean angle of attack has little effects on the time-averaged thrust coefficient and the propulsive efficiency, and, thus, can be ignored in the optimization process of the mean thrust and efficiency. However, it has important effects on the distribution of the instantaneous thrust and input power over oscillation cycle. On the other hand, the oscillation motion has a significant effect on the gradient of the time-averaged lift coefficient with respect to the mean angle of attack.

References

[1]Theodorsen, T., "General theory of aerodynamic instability and the mechanism of flutter," NACA REPORT No. 496, May 1934.

[2]Garrick, I. E., "Propulsion of a flapping and oscillating airfoil," NACA REPORT No. 567, May 1936.

[3]Ho, C.-M. and Chen, S.-H., "Unsteady wake of a plunging airfoil," *AIAA Journal*, Vol. 19, 1981, pp. 1492–1494.

[4]Jones, K. D., Dohring, C. M., and Platzer, M. F., "Experimental and computational investigation of the Knoller-Betz effect," *AIAA Journal*, Vol. 36, 1998, pp. 1240–1246.

[5]Anderson, J. M., "Vorticity control for efficient propulsion," Ph.D Thesis, Massachusetts Institute of Technology and Woods Hole Oceanographic Institution, 1996.

[6]Anderson, J. M., Streitlien, K., Barrentt, D. S., and Triantafyllou, M. S., "Oscillating foils of high propulsive efficiency," *J. Fluid Mech.*, Vol. 360, 1998, pp. 41–72.

[7]Neef, M. F. and Hummel, D., "Euler solutions for a finite-span flapping wing," Tech. rep., Conference on fixed, flapping and rotary wing vehicles at very low Reynolds numbers, Univesity of Norte Dame, IN. June 2000.

[8]Isogai, K., Shinmoto, Y., and Watanabe, Y., "Effects of dynamic stall on propulsive efficiency and thrust of flapping airfoil," *AIAA Journal*, Vol. 37, 1999, pp. 1145–1151.

[9]Baldwin, B. S. and Lomax, H., "Thin layer approximating and algebraic model for separated turbulent flows," *AIAA Paper 78-275*, 1978.

[10]Tuncer, I.H. Walz, R. and Platzer, M., "A computational study on the dynamic stall of a flapping airfoi," AIAA Paper 1998-2519, June 1998.

[11]Tuncer, I. H. and Platzer, M. F., "Computational study of flapping airfoil aerodynamics," *J. of Aircraft*, Vol. 37, 2000, pp. 514–520.

[12]Young, J. and Lai, J. C. S., "Oscillation frequency and amplitude effects on the wake of a plunging airofil," *AIAA Journal*, Vol. 42, 2004, pp. 2042–2052.

[13]Fung, K.-Y. and Carr, L. W., "Effects of compressibilty on dynamic stall," *AIAA Journal*, Vol. 29, 1991, pp. 306–308.

[14]McCroskey, W. J., McAlister, K. W., Carr, L. W., Pucci, S. L., Lambert, O., and Indergrand, R., "Dynamic stall on advanced airfoil sections," *Journal of the American Helicopter Society*, Vol. 26, 1981, pp. 40–50.

[15]Cai, J., Tsai, H.-M., Luo, S., and Liu, F., "Stability of vortex pairs over slender conical bodies– theory and numerical computations," AIAA Paper 2004-1072, Jan. 2004.

[16]Liu, F. and Jameson, A., "Multigrid Navier-Stokes calculations for three-dimensional cascades," *AIAA Journal*, Vol. 31, No. 10, October 1993, pp. 1785–1791.

[17]Liu, F. and Zheng, X., "A strongly-coupled time-marching method for solving the Navier-Stokes and k-ω turbulence model equations with multigrid," *J. of Computational Physics*, Vol. 128, 1996, pp. 289–300.

[18]Liu, F. and Ji, S., "Unsteady flow calculations with a multigrid Navier-Stokes method," *AIAA Journal*, Vol. 34, No. 10, Oct. 1996, pp. 2047–2053.

[19]Sadeghi, M., Yang, S., and Liu, F., "Parallel computation of wing flutter with a coupled Navier-Stokes/CSD method," AIAA Paper 2003-1347, Jan. 2003.

[20]Yang, S., Luo, S., Liu, F., and Tsai, H.-M., "Computation of the flows over flapping airfoil by the Euler equations," AIAA Paper 2005-1404, Jan. 2005.

[21]Yang, S., Luo, S., Liu, F., and Tsai, H.-M., "Trailing-edge flow about unstalled plunging airfoil computed by Euler method," Aiaa paper, submitted to 24th AIAA Applied Aerodynamics Conference, San Francisco, CA, 5-8 June, 2006.

[22]Yang, S., Luo, S., Liu, F., and Tsai, H.-M., "Supercritical Flow over Unstalled Plunging Airfoil Computed by Euler Method," AIAA Paper 2006-0293, Jan. 2006.

[23]Turkel, E., "Preconditioning techniques in computational fluid dynamics," *Annu. Rev. Fluid Mech.*, Vol. 31, 1999, pp. 385–416.

[24]Lewin, G. C. and Haj-Hariri, H., "Modelling thrust generation of a two-dimensional heaving airfoil in a viscous flow," *J. Fluid Mech.*, Vol. 492, 2003, pp. 339–362.

[25]Abbott, I. H. and Doenhoff, A. E. V., *Theory of Wing Sections – Including a Summary of Airfoil Data*, Dover, New York, 1959.

[26]McCroskey, W. J. and Pucci, S. L., "Viscous-inviscid interaction on oscillating airfoils in subsonic flow," *AIAA Journal*, Vol. 20, 1982, pp. 167–174.

[27]Fung, Y. C., *An Introduction to the Theory of Aeroelasticity*, Dover, New York, 1993.